Journal of Materials Processing Technology 209 (2009) 5167–5177

Contents lists available at ScienceDirect

Journal of Materials Processing Technology

journal homepage: www.elsevier.com/locate/jmatprotec

Computational modelling of 3D turning: Influence of edge micro-geometry on forces, stresses, friction and tool wear in PcBN tooling

Tugrul Özel*

Department of Industrial and Systems Engineering, Rutgers University, Piscataway, NJ 08854, USA

ARTICLE INFO

Article history:
Received 18 November 2008
Received in revised form 5 February 2009
Accepted 5 March 2009

Keywords:
Computational machining
Finite element method
Variable edge design tool geometry

ABSTRACT

In this paper, computational modelling of 3D turning process in the presence of variable design cutting tool inserts is studied. Turning of alloy steel, AISI 4340, which utilized in high strength mechanical components for automotive and aerospace industry steel with uniform and variable edge design Polycrystalline cubic Boron Nitride (PcBN) inserts is performed. In the experiments chip geometry, forces and tool wear are measured. 3D computational modelling is utilized to predict chip formation, forces, stresses, temperatures and tool wear on uniform and variable edge design tools. Influence of variable edge tooling on resultant pressure-dependent friction has been investigated by utilizing 3D process simulations. Predicted forces are compared with experiments until pressure-dependent shear friction factor is solved. In general, a lower friction concentration is found for variable edge tooling. The temperature and stress distributions and tool wear contours reveal the advantages of variable edge micro-geometry design.

1. Introduction

Machining is still indisputably the most popular manufacturing process in manufacturing of high precision discrete metal parts. Turning of hardened steels into finished parts by eliminating intermediate machining and reducing grinding processes has been a cost-effective method for manufacturing high quality automotive components (Byrne et al., 2003). Besides, hard turning is a more flexible, more environmentally benign and higher throughput alternative to grinding. However, process reliability and surface quality is still considered behind grinding processes due to issues related to geometrically defined cutting tools (Klocke et al., 2005). In hard turning, Polycrystalline cubic Boron Nitride (PcBN) cutting tools with various edge preparations (chamfer, radius, bi-radii oval or waterfall edges—see Fig. 1) are preferred to protect the cutting edge especially around the insert corner (nose) primarily from chipping (Matsumoto et al., 1999; Byrne et al., 2003; M'Saoubi and Chandrasekaran, 2004; Klocke et al., 2005). PcBN tools can withstand the extremely high temperatures but binder material in the polycrystalline tool body fails after cutting temperature exceeds a threshold (usually around 1200 °C). Micro-geometry of the insert also has significant influence upon the surface integrity. Hence edge preparation must be carefully selected for a given application because it may generate subsurface damage and result in highly tensile residual stress on the surface of the machined workpiece (Klocke et al., 2005; Klocke and Kratz, 2005; Denkena et al., 2005; Özel et al., 2005). Heat generation during hard turning and heat distribution along the insert corner is also affected by micro-geometry due to change in work material flow around the cutting edge (Klocke and Kratz, 2005). For example, a chamfered face provides excessive negative angle to the cutting action and results in high heat generation. PcBN tools rapidly wear out during hard turning at high cutting speeds mainly due to dissolving binder material at attained high cutting temperatures (Byrne et al., 2003; Klocke and Kratz, 2005; Denkena et al., 2005). Flank wear occurs at flank face of the minor cutting edge where as crater wear mostly forms on the rake face near the major cutting edge (Poulachon et al., 2001; Klocke and Kratz, 2005; Denkena et al., 2005). Often, flank wear is followed by crater wear and catastrophic tool failure (chipping). In order to improve the productivity and reliability of hard turning processes, optimum design of micro-geometry for the PcBN inserts must be accomplished.

2. Micro-geometry edge design

It is without a doubt that the design of the cutting edge micro-geometry becomes important to achieve high performance in machining with PcBN cutting tools. For high efficiency material removal with a corner (nose) radius (r_ε) insert, a constant uncut chip thickness to edge radius ratio ($\lambda = t_u/r_\beta$) should be maintained along the engagement area between the insert and the workpiece. However, most edge preparations are applied uniformly all around the corner radius of the PcBN inserts. Uniform edge design hinders the potential of high performance cutting since it does not provide a

* Tel.: +1 732 445 1099; fax: +1 732 445 5467.
E-mail address: ozel@rutgers.edu.

0924-0136/$ – see front matter © 2009 Elsevier B.V. All rights reserved.
doi:10.1016/j.jmatprotec.2009.03.002

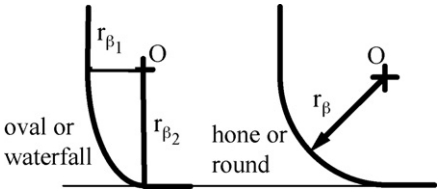

Fig. 1. Waterfall ($r_{\beta 1}$:$r_{\beta 2}$) and round (r_β) hone micro-geometry edge design (Özel et al., 2008).

constant uncut chip thickness to edge ratio (λ) along the insert corner in all engagement conditions. A uniform edge micro-geometry along the insert corner creates a very low uncut chip thickness to edge radius ratio at the minor cutting edge where uncut chip thickness becomes very small. This causes more ploughing than shearing at the minor cutting edge resulting in excessive stress and heat built-up, hence rapid tool wear. A variable edge micro-geometry along the insert corner as illustrated in see Fig. 2 has the potential to reduce the stress and heat built-up and enable hard turning at higher cutting speeds and feeds with less tool wear.

This explanation requires in-depth investigation to exploit full potential of the variable micro-geometry edge design inserts in various machining applications. For this purpose, Özel et al. (2008) investigated the influence of variable edge micro-geometry insert edge preparation in hard turning and presented predicted temperature and tool wear values to compare machining performance between uniform and variable edge designs using finite element-based process simulations. Experimental work and finite element analysis presented in this paper is the continuation of this work and the investigations have been extended to understand the influence of uniform and variable micro-geometry edge design upon chip formation, tool–chip contact friction, tool stresses and tool damage.

While uniform edge preparation (chamfer or hone radius) strengthens tool cutting edge, it makes cutting less efficient especially when the ratio of uncut chip thickness to tool radius decreases. This is especially true when friction factor increases with decreasing uncut chip thickness to edge radius ratio as supported by experimental and analytical work in mechanics of high speed cutting with curvilinear tools (Karpat and Özel, 2008a). The work material is trapped near the end of the uncut chip geometry along the corner radius. Inefficient cutting results in increased strains in the workpiece which in turn increases mechanical and thermal loads and results in high temperatures. Fig. 2 demonstrates the chip load of a uniform edge insert during cutting. The thickness of the chip varies from a maximum value, which is equal to feed (f), to a minimum value on the tool's corner radius. A CAD model of a variable edge design tool insert is given in Fig. 3. It can be seen that edge radius at point A is greater than that of at points B and C. The edge radii at points A, B and C are noted as $r_{\lambda A} > r_{\beta B} > r_{\beta C}$.

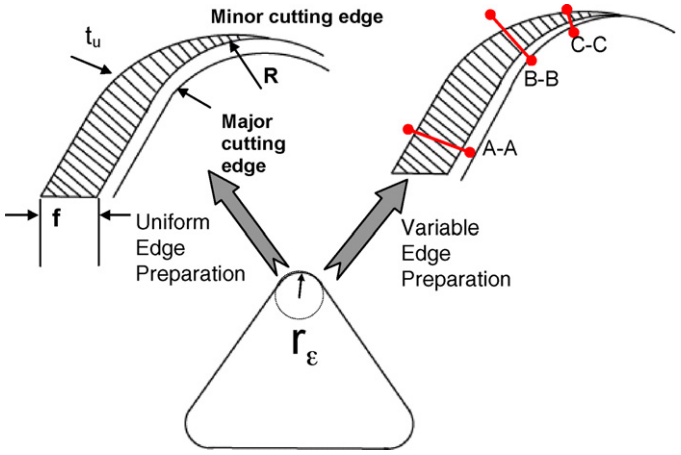

Fig. 2. Uniform vs. variable micro-geometry design (Özel et al., 2008).

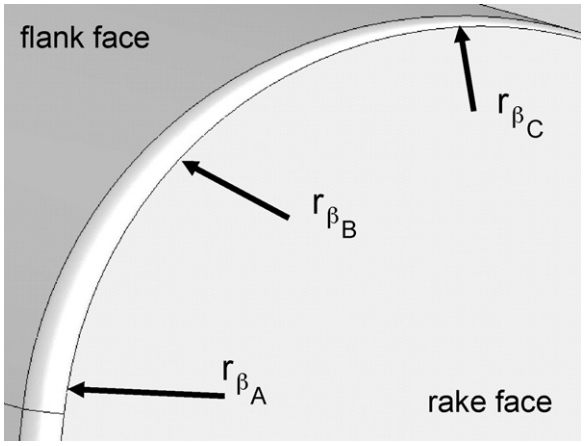

Fig. 3. CAD model of the variable hone edge design (Özel et al., 2008).

In Fig. 2, Section A–A of which is major (leading) cutting edge, uncut chip thickness is greater than the edge radius which indicates regular cutting. In Section B–B, at the end of the leading edge, the uncut chip thickness is equal to the edge radius where the rubbing action becomes more dominant than shearing. In Section C–C, at the minor (trailing) cutting edge, the edge radius is larger than the thickness of the uncut chip and work material is rubbed against the workpiece. This rubbing action which results in increased stresses and temperatures on the tool and workpiece surfaces is believed to hinder the performance of the tool.

3. Experimental work

In this study, experiments presented in Özel et al. (2008) are utilized. These experiments were conducted in turning of annealed and hardened AISI 4340 steel (40 HRC) using PcBN inserts (50%CBN + 40%TiC + 6%WC + 4%Al(N, B2)) with four different micro-geometries (uniform chamfer with 0.1 mm chamfer height and 20° angle, uniform hone with 50 μm (and 40 μm) edge radius, waterfall (WF) hone with $r_{\beta 1}$ = 30 μm and $r_{\beta 2}$ = 60 μm radii (WF 30:60), variable hone edge with $r_{\beta A}$ = 50 μm, $r_{\beta B}$ = 10 μm (Var. 50) radii (see Fig. 4) were considered. Images of the insert micro-geometry were obtained by using Field Emission Scanning Electron Microscopy (FESEM) at the Department of Materials Science and Engineering of Rutgers University.

Turning of cylindrical bar specimens (diameter of 71 mm and length of 305 mm) is illustrated in Fig. 5. Solid top PcBN inserts (TNG-423) were used with a Kennametal MTGNR-123B right hand tool holder that provided 0° lead, −5° side rake, and −5° back rake angles. It must be noted that the corner radius of the PcBN inserts (TNG-423) used in experiments is r_ε = 1.2 mm which means that the cutting has been performed by the corner radius of the inserts ($d < r_\varepsilon$). Experimental cutting conditions are given in Table 1. The cutting forces were measured with a three-component force dynamometer (Kistler Type 9121) mounted on the turret disk of the CNC lathe. The charge signal generated at the dynamometer was amplified using charge amplifiers (Kistler Type 5814B1), acquired and sampled by using data acquisition PCMCIA card and Kistler DynoWare software on a laptop computer. Tool micro-geometry was inspected with Keyence VHX-600 digital microscope to observe the wear and damage behavior.

In the experiments, the force measurements were replicated three times. The averages of the measured forces for each insert in machining of AISI steel at 20 HRC hardness are shown in

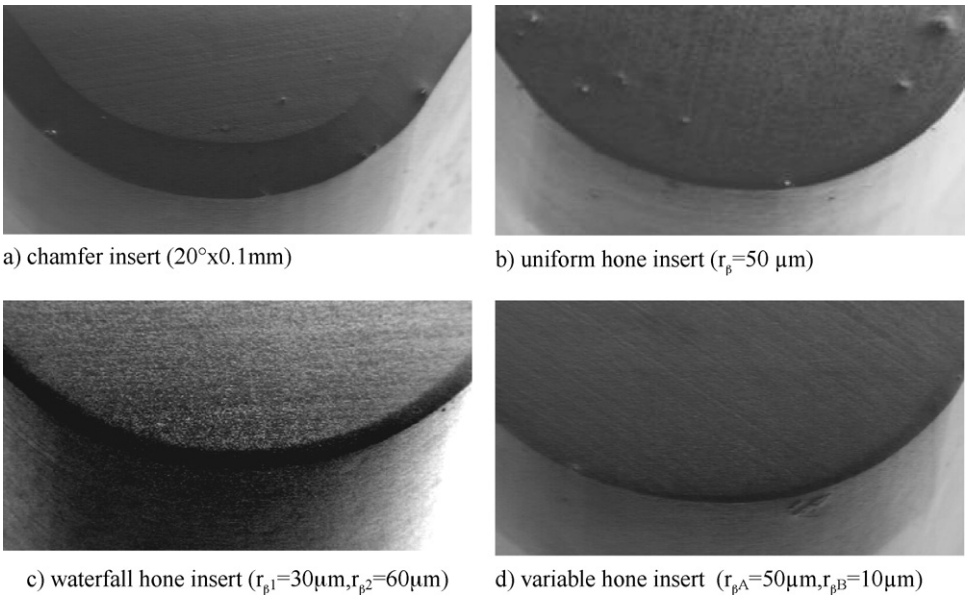

Fig. 4. Images of PcBN inserts at 50 times magnification obtained with FESEM.

Table 1
Experimental cutting conditions for turning AISI 4340 steel.

Hardness HRC	Cutting conditions	Edge micro-geometry
20	V = 125 m/min, f = 0.15 mm/rev, d = 1 mm	Chamfer, hone 50 μm, Var. hone 50 μm, WF 30:60 μm
20	V = 125 m/min, f = 0.10 mm/rev, d = 1 mm	Chamfer hone 50 μm, Var. hone 50 μm, WF 30:60 μm
20	V = 175 m/min, f = 0.15 mm/rev, d = 0.5 mm	Chamfer hone 50 μm, Var. hone 50 μm, WF 30:60 μm
40	V = 300 m/min, f = 0.15 mm/rev, d = 1 mm	Chamfer hone 40 μm, Var. hone 50 μm, WF 30:60 μm

Fig. 6. It should be noted that measured force values with replications revealed ±5% variations and only the force averages of these replications are given in Fig. 6. The effect of edge micro-geometry is apparent on measured radial (thrust) forces (F_t). For the cutting condition of V = 125 m/min, f = 0.15 mm/rev, d = 1 mm, waterfall hone edge with 30:60 μm edge radii yielded the lowest radial forces (F_t) followed by variable hone 50 μm edge radius. These two variable edge design produced higher tangential (cutting) forces (F_c) than other edge micro-geometry designs. This result may imply that more efficient cutting has been performed due to variable edge micro-geometry design that resulted in lower radial forces but slightly higher tangential forces. The ratio of feed to edge radius ($f/r_{\beta A}$) was 3 in that cutting condition. Decreasing feed rate (f = 0.1 mm/rev) resulted in lower tangential forces. In this cutting condition (Fig. 5b), variable honed insert ($r_{\beta A}$ = 50 μm, $r_{\beta B}$ = 10 μm) yielded the lowest radial force. Variable micro-geometry edge designs performed well in this condition. Largest radial (thrust) force was measured when turning with the chamfered insert whereas variable honed insert resulted in lowest radial force. Tangential (cutting) and axial (feed) forces (F_z) are measured to be almost the same for all four inserts at higher feed rate (f = 0.15 mm/rev). However, at lower feed rate (f = 0.1 mm/rev) waterfall hone (30:60 μm) and chamfer micro-geometry resulted largest tangential (cutting) forces (Fig. 5b).

Measured forces in experimental conditions at machining of AISI steel at 20 HRC hardness conditions shown in Table 1 are fitted in log-linear models as function of cutting conditions and micro-geometry design parameters ($r_{\beta1}$ and $r_{\beta2}$). Thrust, feed and cutting force expressions are given in Eqs. (1)–(3) with R-sq = 96.1%, 99.5%, and 99.8% respectively.

$$F_t = 3789.5 d^{0.258} V^{-0.437} f^{0.466} r_{\beta1}^{0.0829} r_{\beta2}^{0.199} \quad (1)$$

$$F_z = 2670.4 d^{1.14} V^{-0.327} f^{0.327} r_{\beta1}^{0.0478} r_{\beta2}^{0.112} \quad (2)$$

$$F_c = 6568 d^{0.895} V^{-0.160} f^{0.695} r_{\beta1}^{0.0145}\ r_{\beta2}^{0.0053} \quad (3)$$

These expressions could provide practical solution to process design problem for machining AISI 4340 steel with hardness around 20 HRC. It should be noted that the nose radius of the insert (r_ε = 1.2 mm) was kept constant in this study. Related parameters

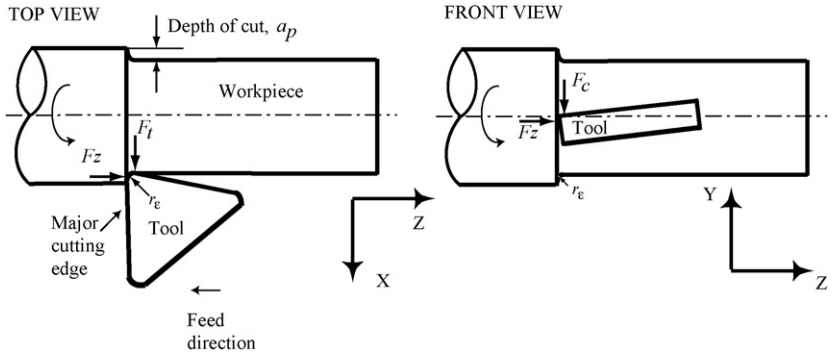

Fig. 5. Illustration of forces in 3D cylindrical turning.

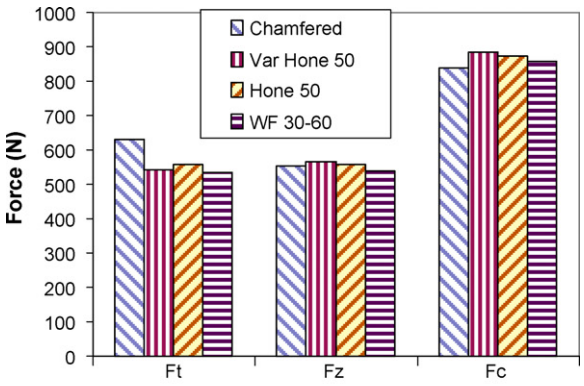

(a) V=125 m/min, f=0.15 mm/rev, d=1 mm

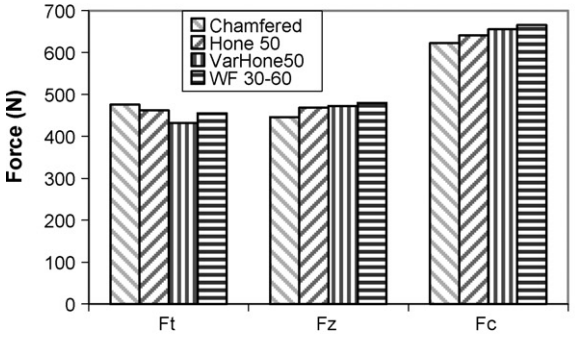

(b) V=125 m/min, f=0.1 mm/rev, d=1 mm.

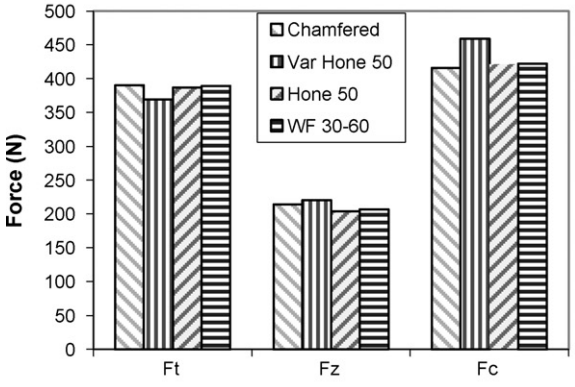

(c) V=175m/min, f=0.15 mm/rev, d=0.5mm

Fig. 6. Measured forces in turning of AISI 4340 steel (20 HRC).

for the variable micro-geometry edge design ($r_{\beta A}$, $r_{\beta B}$, $r_{\beta 1}$, $r_{\beta 2}$) can also be selected to minimize force components. Measured forces in machining hardened AISI 4340 steel will be utilized in determining friction factors for the micro-geometry inserts. They will also be utilized to validate computational models for 3D machining using uniform and variable micro-geometry inserts. Then, computational models will be used to investigate tool temperatures and stresses and tool wear and compare the cutting performance using uniform and variable micro-geometry PcBN inserts.

4. Computational modelling of 3D turning

Mechanics and dynamics of machining hard metals using tools with uniform edge preparations (chamfered, honed, waterfall hone etc.) has been investigated experimentally and analytically in several studies (Davies et al., 1997; M'Saoubi and Chandrasekaran, 2004; Ren and Altintas, 2000; Karpat and Özel, 2008a; Karpat and Özel, 2008b). In addition, Finite Element (FE) modelling studies for orthogonal 2D cutting are used to investigate the influence of edge preparation on the process variables such as chip formation, forces, temperatures and stresses (Özel, 2003; Yen et al., 2004; Hua et al., 2005; Chen et al., 2006; Umbrello et al., 2008). Serrated chip formation is also revealed with increasing cutting speed and feed rate in most experimental and FE studies in hard turning (Umbrello et al., 2008; Karpat and Özel, 2008a).

Table 2
Pressure-dependent heat conduction coefficient.

	p (MPa)					
	0	30	180	300	420	600
h (kW m^{-2} K^{-1})	5	18	87	222	410	500

However, FE studies on 3D hard turning are very limited. Ceretti et al. (2000) developed a 3D FE model for turning to predict cutting forces, temperature and stress distributions for the machining of aluminium alloys and low-carbon steels under orthogonal and oblique cutting configurations. Guo and Liu (2002) proposed a 3D FE model for hard turning of AISI 52100 steel using PcBN tools. The model was used to predict the temperature distribution over the cutting edge, the residual stress distribution on the machined surface and cutting forces. Klocke and Kratz (2005) utilized 3D FE modelling to investigate chamfer edge design in wiper inserts particularly identifying high temperature zones "hot-spots" on the tool face. Aurich and Bil (2006) introduced 3D Finite Element modelling for segmented chip formation. Karpat and Özel (2007) presented experimental and simulation results for 3D FEA of hard turning of AISI H13 steel using chamfered and honed inserts. Özel et al. (2008) have presented 3D Finite Element modelling for hard turning with variable micro-geometry inserts. Attanasio et al. (2008) presented 3D FE simulations for tool wear predictions in turning.

In this study, a Finite Element modelling software (DEFORM 3D) is used to study the effects of uniform and variable micro-geometry edge design on process variables. The FEM software DEFORM 3D is based on an implicit Lagrangian computational routine with continuous adaptive remeshing. The workpiece is modelled as rigid-perfectly plastic material where the material constitutive model of this deformable body is represented with Johnson–Cook material model (see Eq. (4)) where A = 1504 MPa, B = 569 MPa, n = 0.22, C = 0.003, m = 0.9, T_{melt} = 1426 °C are the parameters for AISI 4340 steel as given by Gray et al. (1994).

$$\bar{\sigma} = [A + B(\bar{\varepsilon})^n]\left[1 + C\ln\left(\frac{\dot{\bar{\varepsilon}}}{\dot{\bar{\varepsilon}}}\right)\right]\left[1 - \left(\frac{T - T_0}{T_{melt} - T_0}\right)^m\right] \quad (4)$$

Workpiece is represented by a curved model with 70 mm diameter which is consistent with the experimental conditions. Only a segment (15°) of the workpiece was modelled in order to keep the size of mesh elements small. Workpiece model includes 200,000 elements. The bottom surface of the workpiece is fixed in all directions. The cutting tool is modelled as a rigid body which moves at the specified cutting speed by using 125,000 elements. A very fine mesh density is defined at the tip of the tool and at the cutting zone to obtain fine process output distributions. The

Table 3
Thermo-mechanical properties of work and tool materials.

	AISI 4340	PcBN
Density (kg m^{-3})	7850	4280
Modulus of elasticity (GPa)	205	587
Poisson's ratio	0.29	0.13
Specific heat (J kg^{-1} K^{-1})	475	750
Thermal conductivity (W m^{-1} K^{-1})	44.5	44
Thermal expansion (μm m^{-1} K^{-1})	12.3	4.7

Table 4
The effect of friction factor on process outputs.

Micro-geometry Edge design	Friction model	F_t (N)	F_c (N)	F_z (N)	Tool (°C)
Chamfer (20° × 0.1 mm)	$\mu = 0.4$	362	750	290	384
	$m = 0.5$	311	660	220	708
	$m = 0.75$	299	700	236	1020
	$\boldsymbol{m_1(p)}$	**386**	**775**	**335**	**853**
Uniform hone, $r_\beta = 40$ μm	$m = 0.5$	294	753	251	824
	$\boldsymbol{m_1(p)}$	**324**	**675**	**336**	**664**
	$m_2(p)$	354	835	276	623
	$m_3(p)$	354	835	276	623
	$m_5(p)$	248	472	190	589
Waterfall, $r_{\beta1} = 30$ μm, $r_{\beta2} = 60$ μm	$m = 0.3$	342	782	225	836
	$m = 0.7$	353	816	271	1120
	$\boldsymbol{m_1(p)}$	**360**	**690**	**310**	**724**
	$m_3(p)$	381	842	280	680
	$m_5(p)$	277	560	205	691
Var. hone, $r_{\beta A} = 50$ μm, $r_{\beta B} = 10$ μm	$m = 0.5$	340	786	236	839
	$m_1(p)$	390	800	352	693
	$m_2(p)$	247	648	220	583
	$\boldsymbol{m_3(p)}$	**285**	**690**	**258**	**638**
	$m_4(p)$	231	677	215	596

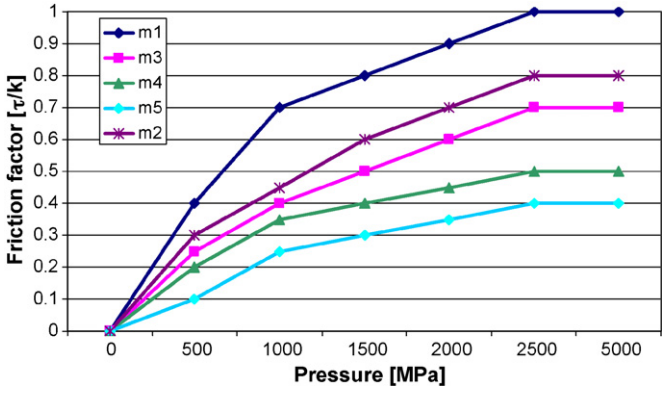

Fig. 7. Pressure-dependent friction factor ($m = \tau/k$).

minimum element size for the workpiece and tool mesh was set to 0.025 mm and 0.009 mm respectively.

Thermal boundary conditions are defined accordingly in order to allow heat transfer from workpiece to cutting tool. Heat conduction to the tool at high contact pressure is higher. Therefore, a heat conduction coefficient, h, is defined as a function of pressure (Rosochowska et al., 2003) is used in this study as given in Table 2. Other thermo-mechanical properties are given in Table 3.

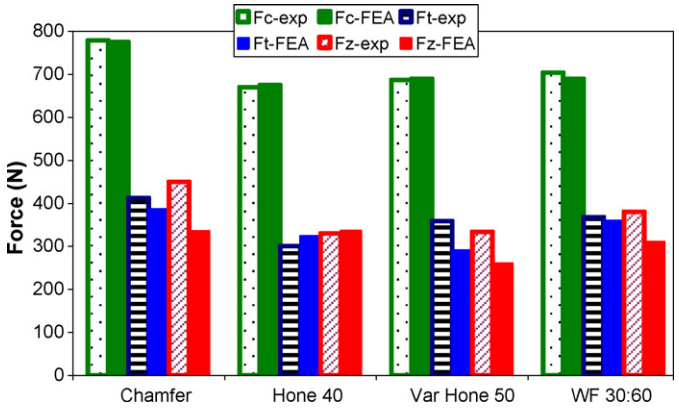

Fig. 8. Comparison of measured and simulated forces (AISI 4340 steel, 40 HRC, $V = 300$ m/min, $f = 0.15$ mm/rev, $d = 1$ mm).

3D computational modelling is utilized to predict chip formation, forces, temperatures and tool wear on uniform and variable edge design tools. All simulations were run at the same cutting condition ($V = 300$ m/min, $f = 0.15$ mm/rev, $d = 1$ mm) for machining of AISI 4340 steel at 40 HRC hardness.

4.1. Influence of variable tool geometry on friction

Friction in metal cutting is found complex due to the different level of contact conditions exist along the tool–chip contact area. This complexity increases when tool inserts with micro-

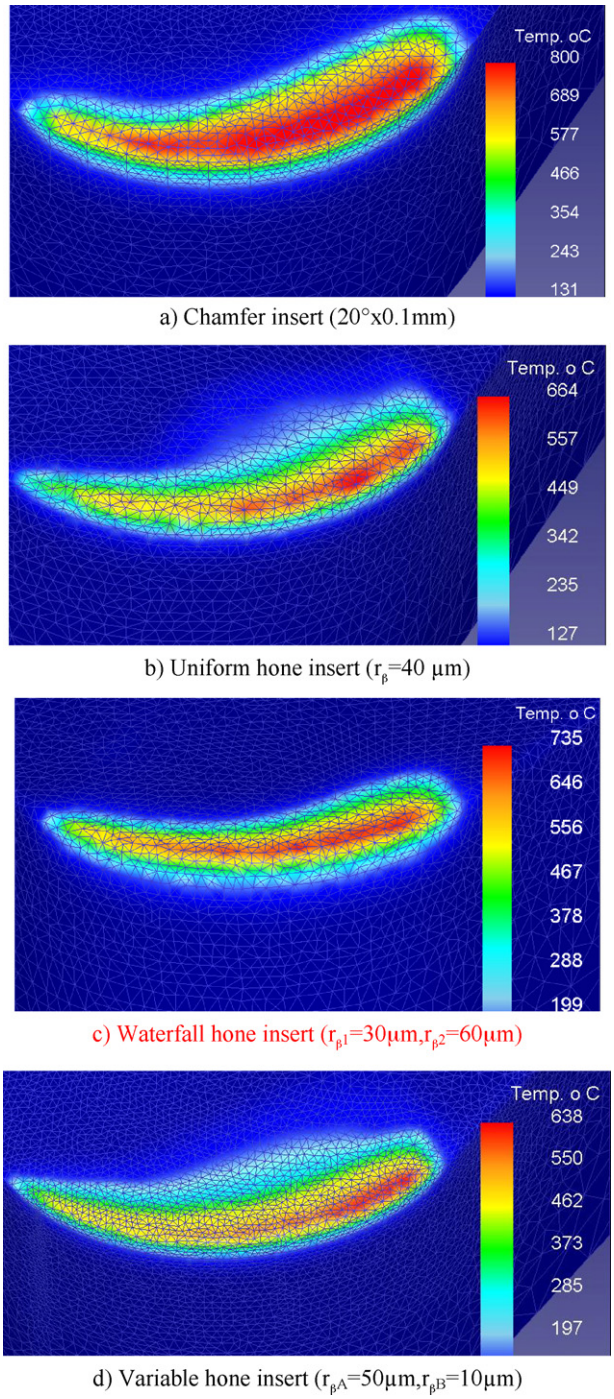

Fig. 9. Temperature distributions simulated for machining with various insert micro-geometries (AISI 4340 steel, 40 HRC, $V = 300$ m/min, $f = 0.15$ mm/rev, $d = 1$ mm).

edge geometry are used in machining. Tool micro-geometry often times increases friction due to increased effective rake angle at the tool tip. Chamfered micro-geometry reveals highest friction with effective rake angles as high as negative 30°. Waterfall hone micro-geometry provides smooth transition from a high effective negative rake to tool rake angle hence eases the normal pressure gradient hence friction factor along the micro-geometry.

In 3D FE modelling, constant shear friction factor, m, Coulomb friction, μ, and pressure-dependent shear friction factor, m (p), have been benchmarked to identify the friction between micro-geometry tool and workpiece as shown in Table 4. Coelho et al. (2007) suggested 0.35 as Coulomb friction for PcBN vs. steel, however no other reliable friction data exist for to be employed in 3D FE modelling of machining. Constant friction models may not represent the sophisticated contact conditions exist in the 3D engagement of the micro-geometry tool edge and the workpiece. On the other hand, friction zones are also difficult to be implemented in 3D problems. Therefore, pressure-dependent shear friction factor approach as a variable friction model and constant shear friction factor are benchmarked in the FE simulations. Variable friction factors are represented as function of contact pressure (local normal stress), m (p), as given in Fig. 7. Also, FE simulation results of predicted forces and tool maximum temperature for various friction models and values during calibration stage are given in Table 4. In general, pressure-dependent shear friction resulted in best force predictions (highlighted as bold).

A simple trial-and-error approach is used during fine-tuning friction models for calibrating FE simulation outputs. Predicted forces are compared with experiments until pressure-dependent shear friction factor is fine-tuned. Then influence of variable edge tooling on resultant pressure-dependent friction has been investigated by utilizing 3D process simulations. In general, a lower friction concentration is found for variable edge tooling. Especially, a reduced shear friction was observed in variable hone micro-geometry PcBN insert.

For machining with chamfered, uniform hone and waterfall inserts, variable friction factor model m_1 (p) found most suitable whereas for machining with variable hone micro-geometry insert variable friction factor model m_3 (p) resulted the closest force predictions to the experiments. The comparison of experimental and simulated forces (F_c, cutting force; F_t, thrust force and F_z, feed force) are shown in Fig. 8. The simulated cutting forces are found to be in close agreements with the experimental ones.

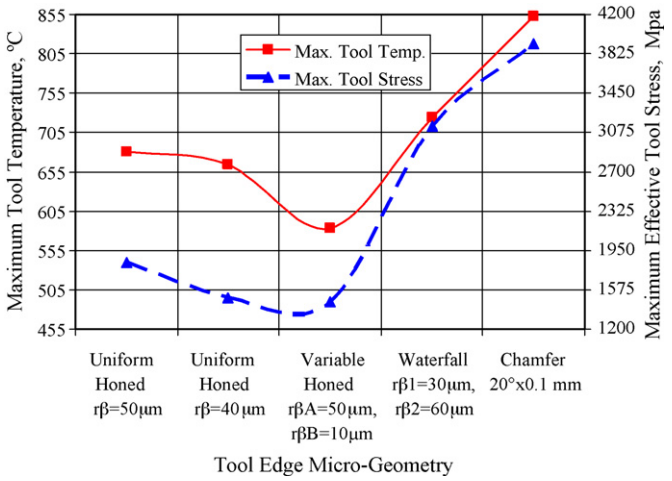

Fig. 10. Influence of micro-geometry on maximum tool temperatures and effective stresses (AISI 4340 steel, 40 HRC, V = 300 m/min, f = 0.15 mm/rev, d = 1 mm).

4.2. Influence of variable micro-geometry on temperature fields

Predicted temperature distributions on the tool for selected micro-geometry inserts are shown in Fig. 9. Temperature distri-

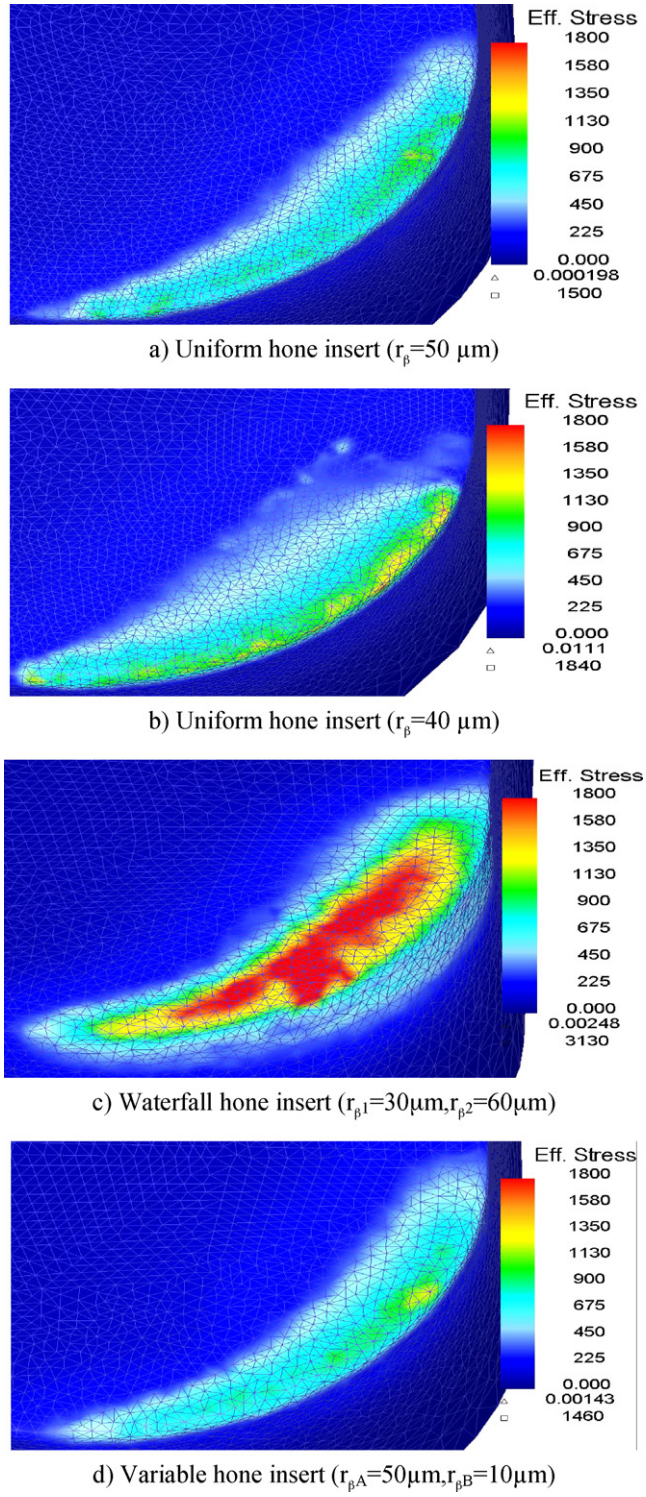

Fig. 11. Tool stress distributions simulated for machining with inserts with various micro-geometries (AISI 4340 steel, 40 HRC, V = 300 m/min, f = 0.15 mm/rev, d = 1 mm).

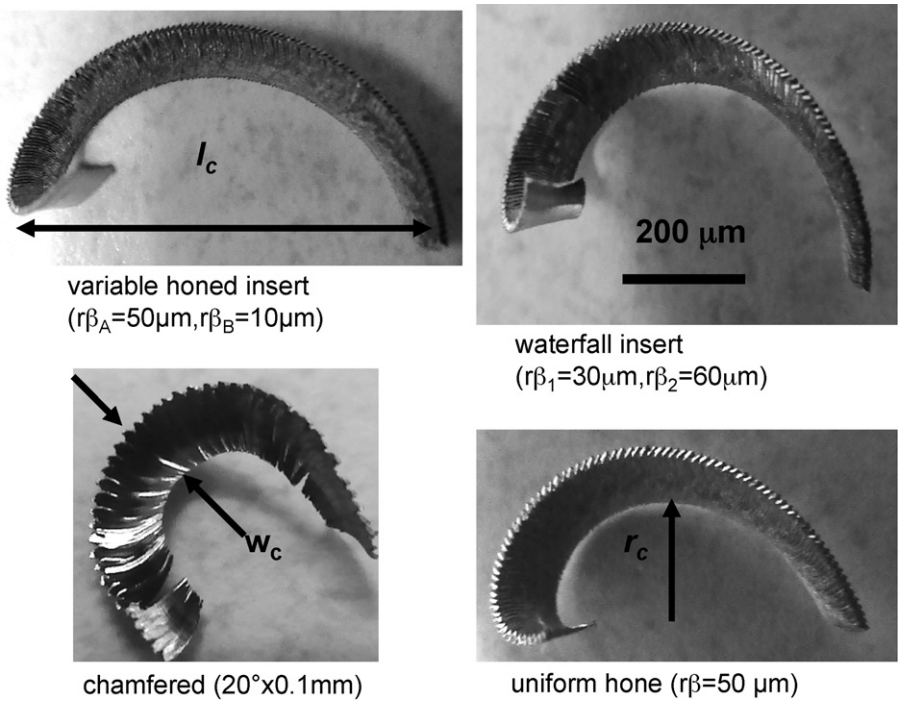

Fig. 12. Effects of micro-geometry on chip geometry (AISI 4340 steel, 40 HRC, V = 300 m/min, f = 0.15 mm/rev, d = 1 mm).

butions depict that smallest hot zone formed on the variable honed insert and maximum temperatures of 853 °C, 724 °C, 680 °C, 664 °C and 626 °C were predicted for uniform chamfered (20° × 0.1 mm), uniform waterfall hone ($r_{\beta1}$ = 30 μm, $r_{\beta2}$ = 60 μm), uniform hone (r_β = 50 μm), uniform hone (r_β = 40 μm) and variable hone ($r_{\beta A}$ = 50 μm, $r_{\beta B}$ = 10 μm) inserts respectively as shown in Fig. 10. Due to the more uniform uncut chip thickness to the edge radius ratio along the variable micro-geometry insert, the cutting temperature at the same cutting condition is found to be significantly lower than other uniform micro-geometry (chamfer, hone and waterfall hone) inserts. In addition, the heat is seen more uniformly distributed along the cutting edge of the variable micro-geometry insert.

4.3. Influence of variable micro-geometry on tool stresses

In order to compute the effective stresses exerted on the inserts, a finite element routine was implemented and tool was modelled as elastic object and the chip load predicted from FE simulations was released over the insert body. This approach has revealed effective stress distributions on the insert with various micro-geometries as shown in Fig. 11. Maximum effective stresses of 3920 MPa, 3130 MPa, 1840 MPa, 1500 MPa and 1460 MPa were predicted for uniform chamfer (20° × 0.1 mm), uniform waterfall hone ($r_{\beta1}$ = 30 μm, $r_{\beta2}$ = 60 μm), uniform hone (r_β = 50 μm), uniform hone (r_β = 40 μm) and variable hone ($r_{\beta A}$ = 50 μm, $r_{\beta B}$ = 10 μm) inserts respectively as shown in Fig. 10. It is apparent that the largest effective stresses occurred with blunt micro-geometry such as uniform chamfer and waterfall hone edge inserts. Although uniform hone inserts pose significant reduction in stress load over the insert edge, the most favourable stress distribution was obtained with variable hone micro-geometry insert.

4.4. Influence of variable micro-geometry on strain fields

Predicted chip geometries and strain fields (see Fig. 12) indicate the effect of micro-geometry edge design on the plastic strain induced on the workpiece. Maximum effective strain of 5.19 mm/mm, 5.08 mm/mm, 4.84 mm/mm, and 3.77 mm/mm were predicted for uniform chamfer (20° × 0.1 mm), uniform waterfall hone ($r_{\beta1}$ = 30 μm, $r_{\beta2}$ = 60 μm), uniform hone (r_β = 40 μm) and variable hone ($r_{\beta A}$ = 50 μm, $r_{\beta B}$ = 10 μm) inserts respectively. Hence, large edge micro-geometry insert has induced greater effective strain hence greater thermo-mechanical load to the workpiece. This creates higher heat generation and higher temperatures on the tool cutting edge. This observation indicates that variable micro-geometry may have the least plastic damage on the machined surface which may be favourable for surface integrity. This claim deserves further investigations about the influence of insert edge micro-geometry upon machined surface integrity in hard turning.

4.5. Influence of variable micro-geometry on chip formation

Influence of micro-geometry edge preparation on the chip formation has also been investigated. The chip morphology and

Table 5
Measured and predicted chip dimensions.

Micro-geometry edge design	Measured w_c (mm)	Predicted w_c (mm)	Measured l_c (mm)	Predicted l_c (mm)	Measured r_c (mm)	Predicted r_c (mm)
Chamfer (20° × 0.1 mm)	0.25	0.3	2.5	2.27	0.5	0.65
Variable hone ($r_{\beta A}$ = 50 μm, $r_{\beta B}$ = 10 μm)	0.24	0.28	2.2	2.3	1.5	1.6
Waterfall hone ($r_{\beta1}$ = 30 μm, $r_{\beta2}$ = 60 μm)	0.24	0.27	1.5	1.55	1.2	1.25
Uniform hone (r_β = 40 μm)	0.29	0.39	1.65	1.69	0.7	0.6

dimensions are given in Fig. 13 and Table 5. FEA output images in Fig. 13 were captured at the same cutting time to compare the influence of micro-geometry in chip formation and effective strain distribution. In the turning experiments, the chip flow was observed with the help of a digital camera, the chip flow off the waterfall micro-geometry insert running parallel with the top rake face of the tool. The uniform chamfer insert showed the chip coming vertically off the tool. There was more vibration in turning with chamfer insert, hence chip formation reflected this with some segmentation as shown in Fig. 12. Variable hone micro-geometry insert produced chip flow direction more parallel towards the trailing edge of the insert. The chip thickness was higher at the trailing edge than any other chips produced with all inserts.

Chip formation at the advanced stages of the cutting is also predicted with finite element simulations for selected cases as shown in Figs. 14 and 15. Chip formation images shown in Fig. 15 have been captured in much later cutting time than that of in Fig. 13 to compare the chip shapes and dimensions with the experimental observations.

Predicted chip geometry in chamfer insert was thinner and wider similar to experimental observations. On the other hand, predicted chip geometries for variable hone and waterfall inserts were thicker but shorter in agreement with experimental chip shapes. Experimental results show continuous chip formation with light serration. However, in the case of chamfer insert micro-geometry serration becomes more severe due to higher temperatures and increased effective negative rake angle.

4.6. Influence of variable micro-geometry on tool wear

Fig. 16 shows a typical damage pattern observed in turning of hardened AISI 4340 steel workpiece with micro-geometry PcBN tools. Depth of cut notch wear is seen as the most dominant wear mode in PcBN. This is primarily due to the weakness of PcBN which is stable against diffusion but it fails under shear so that adhesive wear occurs when chip material adhere to the PcBN surface.

In order to understand the influence of variable micro-geometry inserts on tool wear, finite element simulations are utilized to predict tool wear depth and rate. The distributions of the process variables such as effective stresses, temperatures and sliding velocities allow the simulation of the tool wear on the tool rake and flank faces when combined with a tool wear model. The tool wear rate models describe the rate of volume loss on the tool rake and flank faces per unit area per unit time.

There are many different tool wear rate models proposed in literature depending on the type of tool wear i.e. adhesive, diffusive, etc. Among those, the tool wear rate model based on the adhesive wear proposed by Usui et al. (1978), given in Eq. (5), uses interface temperature, normal stress, and sliding velocity at the contact surfaces as inputs and yields tool wear rate for a given location on the tool surface.

$$\frac{dVB}{dt} = c_1 \sigma_n V_s e^{(-c_2/T)} \tag{5}$$

where dVB/dt is volumetric wear rate, c_1 and c_2 are constants, T is temperature, V_s is sliding velocity, and σ_n is normal stress applied to the tool surface.

In this study, the wear constants c_1 and c_2 for PcBN are found to be as $c_1 = 1 \times 10^{-6}$ and $c_2 = 0.9 \times 10^2$ by trial-and-error with FE simulations. It should be noted here that an attempt to 3D tool wear modelling using FEA has been carried out in this work. Calibration and validation of such tool wear models deserves a separate research effort and left as future work.

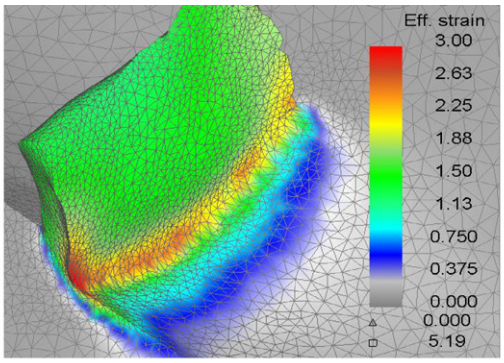

a) Chamfered insert (20°x0.1mm)

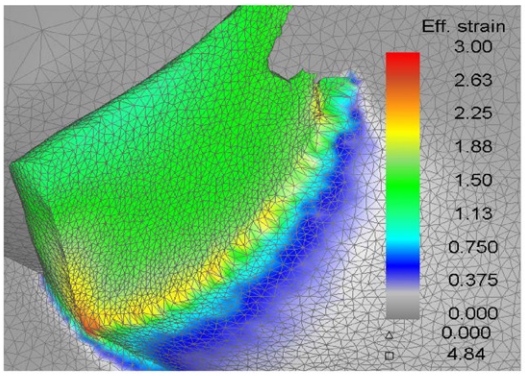

b) Uniform hone insert (r_β=40 μm)

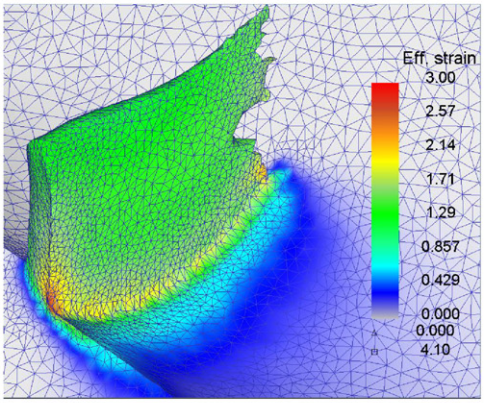

c) Waterfall hone insert ($r_{\beta1}$=30μm,$r_{\beta2}$=60μm)

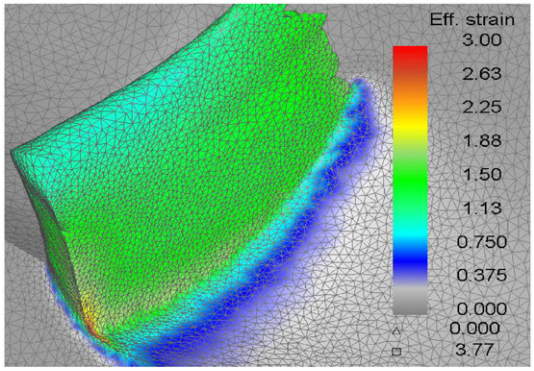

d) Variable hone insert ($r_{\beta A}$=50μm,$r_{\beta B}$=10μm)

Fig. 13. Simulated chip formation and strain fields for various micro-geometry inserts (AISI 4340 steel, 40 HRC, V = 300 m/min, f = 0.15 mm/rev, d = 1 mm) after cutting time of 0.5 ms.

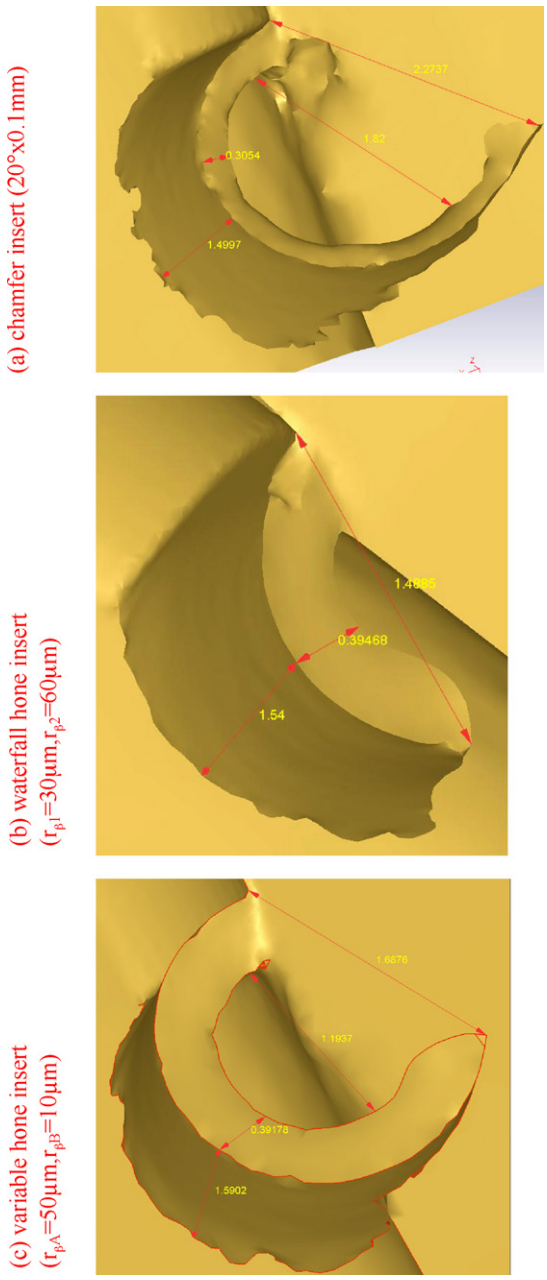

Fig. 14. Predicted chip geometries (AISI 4340 steel, 40 HRC, $V = 300$ m/min, $f = 0.15$ mm/rev, $d = 1$ mm).

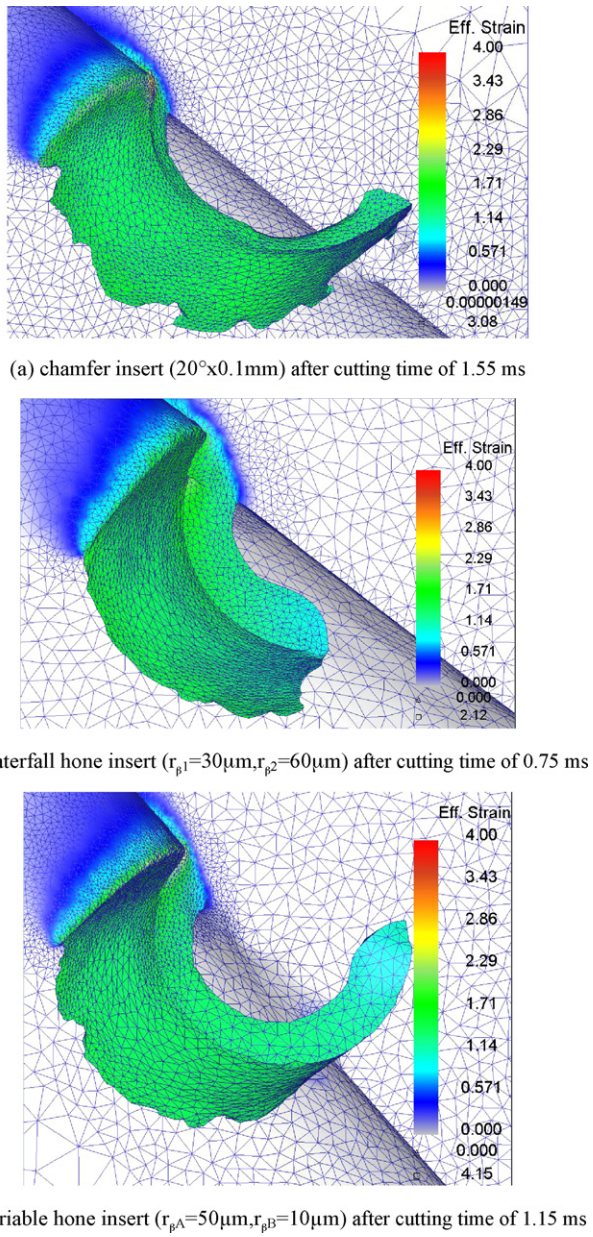

Fig. 15. Predicted strain distributions in the chip and workpiece (AISI 4340 steel, 40 HRC, $V = 300$ m/min, $f = 0.15$ mm/rev, $d = 1$ mm).

Simulated total wear depth in machining with various micro-geometry inserts are shown in Fig. 17. Total wear depth of 11.3 μm, 7.94 μm, 7.61 μm, and 6.36 μm were predicted after cutting of 1.50 ms for uniform waterfall hone ($r_{\beta 1} = 30$ μm, $r_{\beta 2} = 60$ μm), uniform hone ($r_\beta = 50$ μm), uniform hone ($r_\beta = 40$ μm) and variable hone ($r_{\beta A} = 50$ μm, $r_{\beta B} = 10$ μm) inserts respectively. It can be seen that the variable micro-geometry edge design insert has the lowest total wear depth among all other inserts under the same cutting conditions. Furthermore, Fig. 18 shows the simulated tool wear zones on the tool for uniform chamfer ($20^\circ \times 0.1$ mm), uniform hone ($r_\beta = 40$ μm) and variable hone ($r_{\beta A} = 50$ μm, $r_{\beta B} = 10$ μm) inserts.

It should be noted that the FE simulation and prediction of tool wear depth must be after cutting equal amount of time both in experiments and simulations if no accelerated prediction model is implemented. Therefore, predicted tool wear depths were not compared with experiments but a comparison among predicted (FEA) results are given in the paper. It is observed that the variable micro-geometry edge design has the lowest wear rate under the simulation conditions.

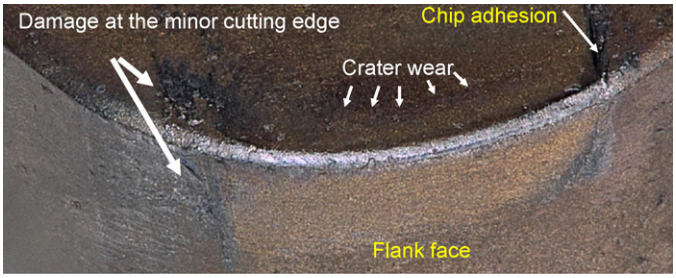

Fig. 16. Image of the worn waterfall honed insert ($r_{\beta 1} = 30$ μm, $r_{\beta 2} = 60$ μm) with wear modes (AISI 4340 steel, 40 HRC, $V = 300$ m/min, $f = 0.15$ mm/rev, $d = 1$ mm).

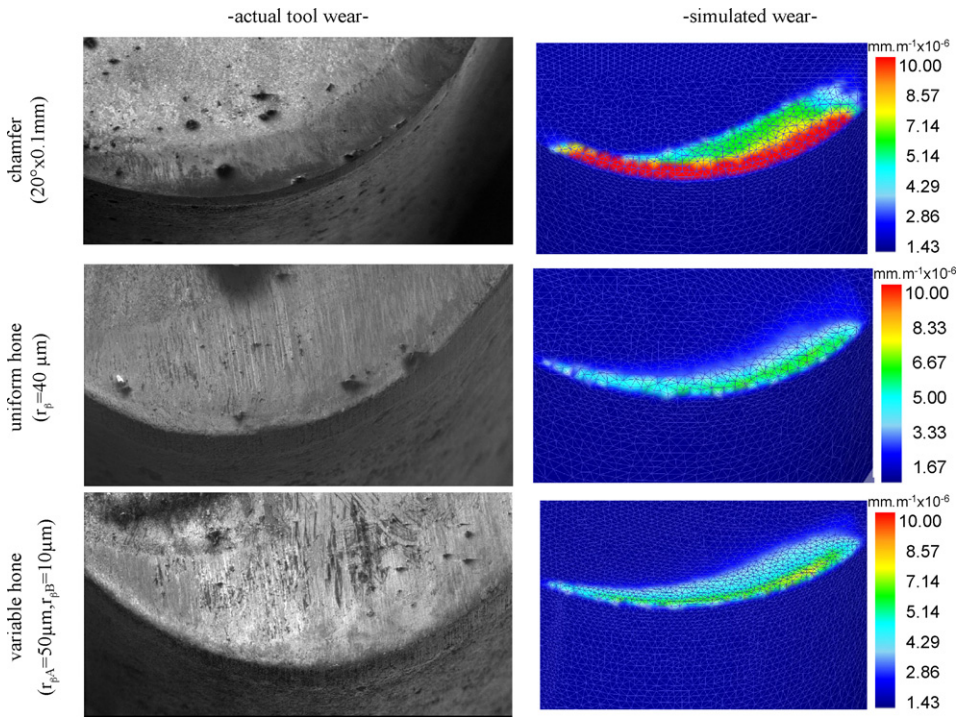

Fig. 17. Comparison of tool wear experiments with simulations after machining of 1.5 ms. (AISI 4340 steel, 40 HRC, V = 300 m/min, f = 0.15 mm/rev, d = 1 mm).

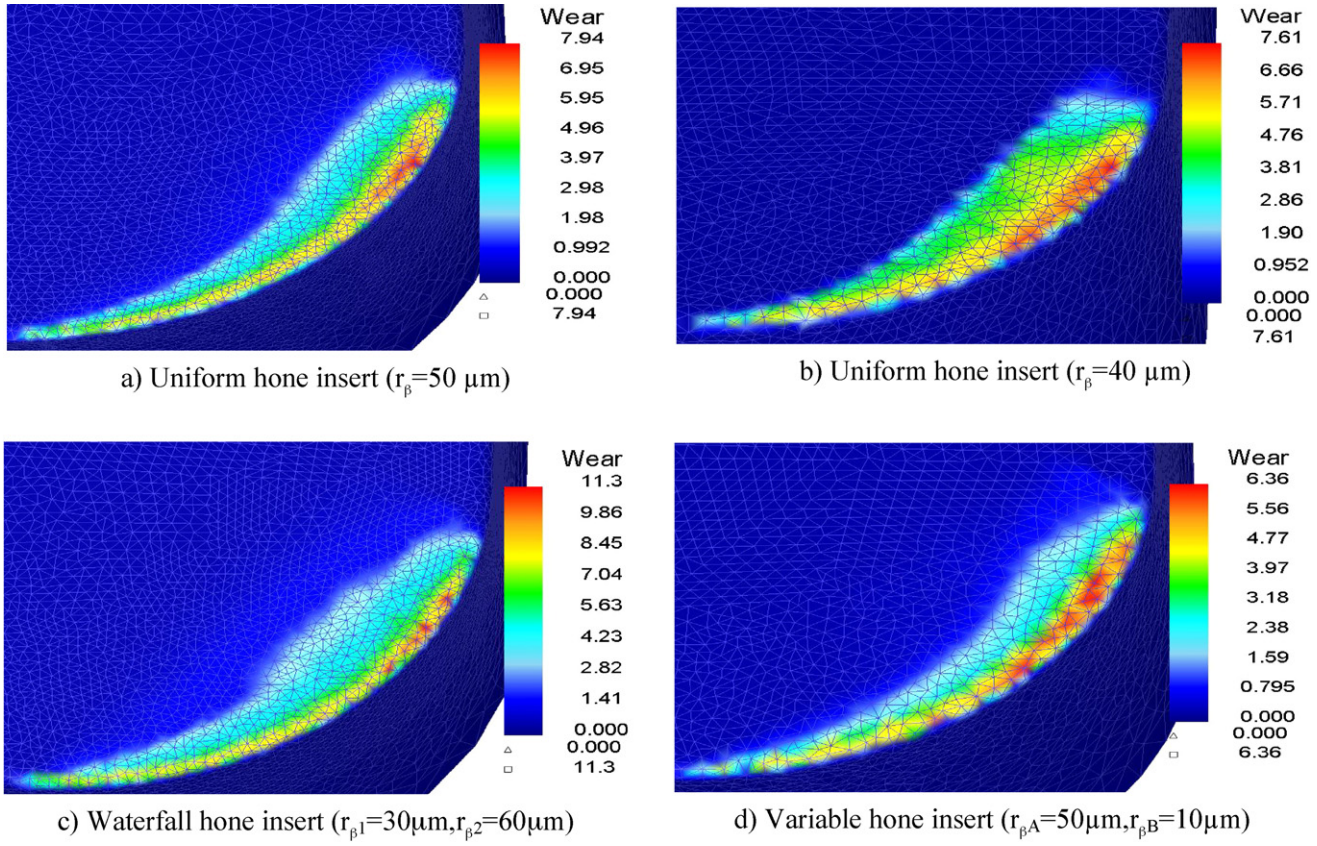

Fig. 18. Simulated total wear depth (µm) in machining with various micro-geometry inserts (AISI 4340 steel, 40 HRC, V = 300 m/min, f = 0.15 mm/rev, d = 1 mm) after cutting of 0.5 ms.

5. Conclusions

In this paper, experimental and FE modelling investigations on 3D turning with uniform and variable edge design PcBN inserts are presented. Cutting experiments and 3D finite element simulations are performed to compare uniform and variable edge preparations. 3D finite element modelling is utilized to predict chip formation, forces, temperatures, stresses and tool wear on uniform and vari-

able edge micro-geometry tools. Predicted forces and tool wear are compared with experiments. These results revealed that the variable edge preparation inserts perform best, followed by uniform honed and uniform waterfall honed shape inserts. It is apparent from the results presented that the variable micro-geometry inserts are favourable for extended performance over uniform counterparts when the variable edge is properly designed for a given cutting condition. Specifically, the following conclusions can be made:

- Variable micro-geometry insert edge design reduces the heat generation and stress concentration along the tool cutting edge significantly. This has implications over improved tool life.
- Variable micro-geometry insert cutting edge induces less plastic strain on the machined workpiece. This outcome may be seen as favourable for improved surface integrity and deserves further investigations on subsurface damage on the machined surfaces.
- Tool wear depth and predicted wear rate is decreased with the use of a variable micro-geometry insert.

Acknowledgements

The author greatly acknowledges Mr. W. Shaffer of Conicity Inc. for providing PcBN inserts with custom micro-geometry, Dr. A.K. Srivastava for discussions and his former student Dr. Y. Karpat for participating in the earlier stages of this study.

References

Attanasio, A., Ceretti, E., Rizzuti, S., Umbrello, D., Micari, F., 2008. 3D finite element analysis of tool wear in machining. CIRP Annals—Manufacturing Technology 57 (1), 61–64.

Aurich, J.C., Bil, H., 2006. 3D finite element modelling of segmented chip formation. Annals of the CIRP 55 (1), 47–50.

Byrne, G., Dornfeld, D., Denkena, B., 2003. Advanced cutting technology. Annals of the CIRP 52 (2), 483–507.

Ceretti, E., Lazzaroni, C., Menegardo, L., Altan, T., 2000. Turning simulations using a three-dimensional FEM code. Journal of Materials Processing Technology 98, 99–103.

Chen, L., ElWardany, T.I., Nasr, M., Elbestawi, M.A., 2006. Effects of edge preparation and feed when hard turning a hot work die steel with polycrystalline cubic boron nitride tools. Annals of the CIRP 55 (1), 88–92.

Coelho, R.T., Ng, E., Elbestawi, M.A., 2007. Tool wear when turning hardened AISI 4340 with coated PcBN tools using finishing cutting conditions. International Journal of Machine Tools and Manufacture 47, 263–272.

Davies, M.A., Burns, T.J., Evans, C.J., 1997. On the dynamics of chip formation in machining hard metals. Annals of the CIRP 46 (1), 25–28.

Denkena, B., Becker, J.C., de Leon-Garcia, L., 2005. Study of the influence of the cutting edge microgeometry on the cutting forces and wear behavior in turning operations. In: Proceedings of the 8th CIRP, International Workshop on Modelling of Machining Operations, Chemnitz, Germany, pp. 503–507.

Gray, G.T., Chen, S.R., Wright, W., Lopez, M.F., 1994. Constitutive equations for annealed metals under compression at high strain rates and high temperatures. Los Alamos National Laboratory Report, LA-12699-MS.

Guo, Y., Liu, C.R., 2002. 3D FEA modeling of hard turning. ASME Journal of Manufacturing Science and Engineering 124, 189–199.

Hua, J., Shivpuri, R., Cheng, X., Bedekar, V., Matsumoto, Y., Hashimoto, F., Watkins, T.R., 2005. Effect of feed rate, workpiece hardness and cutting edge on subsurface residual stress in hard turning of bearing steel using chamfer and hone edge geometry. Materials Science and Engineering A394, 238–248.

Karpat, Y., Özel, T., 2007. 3-D FEA of hard turning: investigation of PCBN cutting tool micro-geometry effects. Transactions of NAMRI/SME 35, 9–16.

Karpat, Y., Özel, T., 2008a. Mechanics of high speed machining with curvilinear tools. International Journal of Machine Tools and Manufacture 49, 195–208.

Karpat, Y., Özel, T., 2008b. Analytical and thermal modeling of high-speed machining with chamfered tools. ASME Journal of Manufacturing Science and Engineering 130, 1–15.

Klocke, F., Brinksmeier, E., Weinert, K., 2005. Capability profile of hard cutting and grinding processes. Annals of the CIRP 54 (2), 557–580.

Klocke, F., Kratz, H., 2005. Advanced tool edge geometry for high precision hard turning. Annals of the CIRP 54 (1), 47–50.

Matsumoto, Y., Hashimoto, F., Lahoti, G., 1999. Surface integrity generated by precision hard turning. Annals of the CIRP 48 (1), 59–62.

M'Saoubi, R., Chandrasekaran, H., 2004. Investigation of the effects of tool micro-geometry and coating on tool temperature during orthogonal turning of quenched and tempered steel. International Journal Of Machine Tools and Manufacture 44 (2–3), 213–224.

Özel, T., 2003. Modeling of hard part machining: effect of insert edge preparation for CBN cutting tools. Journal of Materials Processing Technology 141, 284–293.

Özel, T., Hsu, T.-K., Zeren, E., 2005. Effects of cutting edge geometry, workpiece hardness, feed rate and cutting speed on surface roughness and forces in finish turning of hardened AISI H13 steel. International Journal of Advanced Manufacturing Technology 25, 262–269.

Özel, T., Karpat, Y., Srivastava, A.K., 2008. Hard turning with variable micro-geometry PcBN tools. CIRP Annals—Manufacturing Technology 57, 73–76.

Poulachon, G., Moisan, A., Jawahir, I.S., 2001. Tool-wear mechanisms in hard turning with polycrystalline cubic boron nitride tools. Wear 250, 576–586.

Ren, H., Altintas, Y., 2000. Mechanics of machining with chamfered tools. ASME Journal of Manufacturing Science and Engineering 122, 650–659.

Rosochowska, M., Balendra, R., Chodnikiewicz, K., 2003. Measurements of thermal conductance. Journal of Materials Processing Technology 135, 204–210.

Umbrello, D., Rizzuti, S., Outeiro, J.C., Shivpuri, R., M'Saoubi, R., 2008. Hardness-based flow stress for numerical simulation of hard machining AISI H13 tool steel. Journal of Materials Processing Technology 199 (1–3), 64–73.

Usui, E., Hirota, A., Masuko, M., 1978. Analytical prediction of three dimensional cutting process. Part 3. Cutting temperature and crater wear of carbide tool. Journal of Engineering for Industry 100, 236–243.

Yen, Y.C., Jain, A., Altan, T., 2004. A finite element analysis of orthogonal machining using different tool edge geometry. Journal of Materials Processing Technology 146, 72–81.